Neutron spectroscopy of $4f$ collective magnetic excitations in $R_{2-x}Ce_xCuO_4$ (R=Nd,Pr)

W. Henggeler, T. Chattopadhyay, and B. Roessli
Institut Laue-Langevin, Boîte Postale 156, 38042 Grenoble Cedex 9, France

P. Vorderwisch
Hahn-Meitner-Institut, Glienecker Str. 100, D-14109 Berlin, Germany

P. Thalmeier
Max-Planck-Institut für Physik komplexer Systeme, Dresden, Germany

D. I. Zhigunov and S. N. Barilo
Institute of Physics of Solids and Semiconductors, Belarus Academy of Sciences, 220726 Minsk, Belarus

A. Furrer
Laboratory for Neutron Scattering, Eidg. Technische Hochschule Zürich & Paul Scherrer Institut, CH-5232 Villigen PSI, Switzerland
(Received 22 July 1996; revised manuscript received 30 September 1996)

We have studied the wave-vector dependence of the magnetic excitation spectrum of Nd in $Nd_{2-x}Ce_xCuO_4$ ($x=0,0.13$) and of Pr in $Pr_{1.86}Ce_{0.14}CuO_4$ by inelastic neutron-scattering experiments on single crystals. The results are analyzed with the help of model calculations which are performed in the context of the mean-field random-phase approximation. This enables us to obtain direct information on the coupling constants between the rare-earth ions. The exchange couplings between the Pr ions in $Pr_{1.86}Ce_{0.14}CuO_4$ turn out to be slightly reduced compared to the ones in the undoped parent compound Pr_2CuO_4. In Nd_2CuO_4 we observe a dependence of the coupling constants on the initial and final state that is involved in a crystal-field excitation. Furthermore our results indicate that the interaction of the Nd spins is opposite to the ordering enforced by the Nd-Cu exchange. We argue that this will lead to an instability of the Nd ordering in the Ce-doped systems which might be important for the onset of high γ values. [S0163-1829(97)03302-X]

I. INTRODUCTION

The $R_{2-x}Ce_xCuO_4$ (R=Nd,Pr, $0\leqslant x\leqslant 0.2$) compounds have been the subject of intensive investigations since the discovery of superconductivity in some of these substances.[1,2] The superconducting transition occurs in a narrow doping range ($0.13\leqslant x\leqslant 0.18$) with a highest T_c of $\approx$24 K.[3] For R=Pr, this range has recently been extended down to $x=0.04$.[4] Both systems are well suited for the investigation of fundamental properties of superconductivity due to their simple tetragonal crystal structure where the Cu ions exhibit square-planar coordination to oxygen[5] (see Fig. 1, left). Due to the magnetic moments on Cu and on the rare-earth ions these compounds show a variety of interesting magnetic properties. The ordering of the Cu spins has been studied extensively by magnetic-susceptibility measurements,[6,7] neutron diffraction,[8–23] and μSR experiments.[24,25] In the undoped substances, the Cu spins order at a temperature of about 280 K in a noncollinear[26–29] spin structure with propagation vector $\vec{q}=(1/2,1/2,0)$. For R=Nd, two Cu spin reorientations occur at $\approx$70 and $\approx$30 K. For R=Pr, no such reorientations have been observed with neutrons, in disagreement with μSR measurements where such transitions have been proposed to occur at $\approx$110 and $\approx$40 K. Upon Ce doping, the Cu ordering and spin-reorientation temperatures decrease. No Cu ordering is observed for $x\geqslant 0.14$ for R=Nd and Pr. The Cu spin dynamics in both compounds seem to follow a simple xy model with in-plane nearest-neighbor exchange constants of 130 ± 13 meV for R=Pr (Ref. 30) and 108 ± 6 meV for R=Nd.[31] The xy anisotropy and the biquadratic in-plane exchange are expected to lead to spin gaps[32] which have been observed at about 2 and 6 meV for R=Pr at 10 K and at about 12 and 14 meV for R=Nd at 5 K.[30,33,34]

The rare-earth magnetism on the other hand is essentially different for R=Nd and Pr, respectively. For R=Pr, the crystalline electric-field (CEF) potential decomposes the $J=4$ ground-state multiplet into a singlet ground state (Γ_4), a first excited doublet at 18 meV (Γ_5) and various other excited states around 80 meV ($2*\Gamma_1,\Gamma_2,\Gamma_3,\Gamma_5$).[35–37] The magnetic moment on the Pr site is quenched by the CEF interaction due to the nonmagnetic singlet ground state. The Pr-Cu exchange interaction induces, however, a small moment on Pr.[15] The exchange interaction between the Pr ions leads to a significant dispersion of the Γ_4-Γ_5 CEF excitation.[30] In the Nd compound, we are confronted with a more complicated magnetic behavior. The tenfold degeneracy of the $J=9/2$ ground-state multiplet is split by the CEF potential into a magnetic ground-state doublet ($\Gamma_6^{(1)}$) and four Kramers doublets at 14 meV ($\Gamma_7^{(1)}$), 21 meV ($\Gamma_6^{(2)}$), 27 meV ($\Gamma_7^{(2)}$), and 93 meV ($\Gamma_6^{(3)}$).[36–41] Specific-heat measurements indicated ordering of the Nd spins at a temperature of about 1.5 K.[42–44] However, it is not correct to talk about a Nd ordering temperature. The order of the Nd moments gradually builds up over a large temperature range as revealed by neutron-diffraction[15,45] and x-ray magnetic scattering.[46] This can be explained by a Cu-Nd exchange

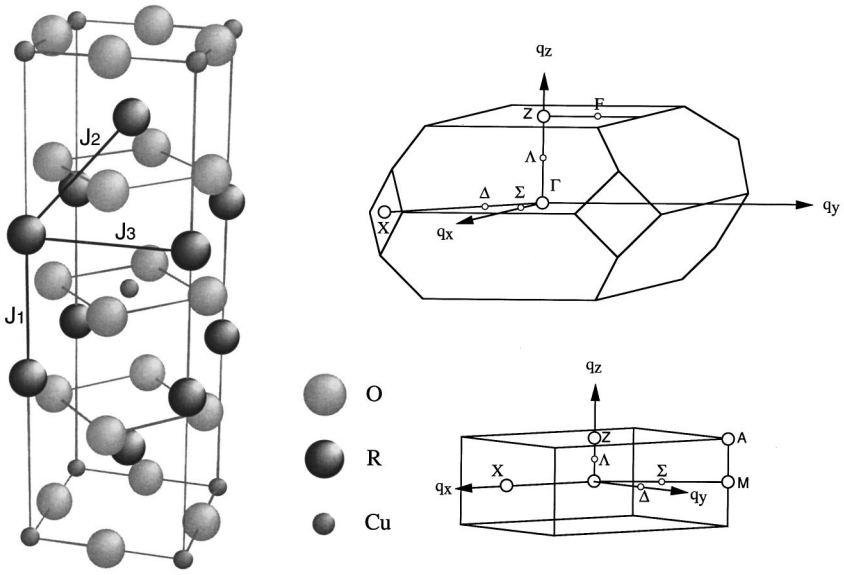

FIG. 1. Left: Crystal structure of R_2CuO_4 with the various R-R exchange constants indicated. Upper right: Brillouin zone of the body-centered-tetragonal lattice. Lower right: Brillouin zone of the tetragonal lattice corresonding to the noncollinear magnetic structure of the Nd spins in Nd_2CuO_4.

interaction which creates a staggered magnetic field at the Nd site. The splitting of the Nd ground-state doublet induced by this magnetic field mainly explains the observed Nd ordering.[47] The Nd-Nd exchange interaction gives only a small contribution to the Nd ordering.[48] In the millikelvin temperature range one moreover observes a hyperfine-induced polarization of the nuclear spins of the ^{143}Nd and ^{145}Nd isotopes.[49]

Upon Ce doping, long-range magnetic order of Nd is observed up to $x=0.13$. Short-range order persists up to $x=0.17$.[50] At low temperatures ($T\leqslant 0.3$ K), specific-heat measurements show for $x\geqslant 0.1$ a large linear term with a huge γ coefficient (4 J K^{-2} Mol^{-1}/Nd for $x=0.2$),[51] which has been interpreted as a heavy-fermion-like behavior. Several models have been developed to explain this behavior.[52–54] The common feature in all these calculations is the assumption that the large linear term arises from the interaction of the strongly correlated electrons in the copper-oxide plane with the Nd ions. In these models, the Nd-Nd interaction has been neglected.

It was the purpose of our study to investigate in detail the magnetic excitation spectrum of the Nd ions in Nd_2CuO_4 in order to obtain information about the Nd-Nd exchange interactions. Moreover we investigated the variation of the exchange interactions upon Ce doping in $Pr_{1.86}Ce_{0.14}CuO_4$ and $Nd_{1.87}Ce_{0.13}CuO_4$. Parts of the results have already been published in two short contributions.[55,56] In Secs. II and III we describe the experiments on a Nd_2CuO_4 single crystal. In Sec. III we moreover show some preliminary results of experiments on Ce-doped $Nd_{1.87}Ce_{0.13}CuO_4$. In Sec. IV we present the results of the determination of the dispersion of the Γ_4-Γ_5 Pr CEF excitation in $Pr_{1.86}Ce_{0.14}CuO_4$. Our findings are discussed in Sec. V.

II. DISPERSION OF THE Nd CEF EXCITATION IN Nd_2CuO_4

The experiments were performed on the triple-axis spectrometers IN8 and IN3 at the high flux reactor of the Institute Laue-Langevin (ILL) in Grenoble, France. On IN8 we used a copper (111) monochromator and a graphite (002) analyzer, both vertically bent. The collimation used was 30′-30′-40′-40′. On IN3 we used a vertically bent copper (111) monochromator and a horizontally bent graphite (002) analyzer. A converging supermirror guide was installed between monochromator and sample. On both instruments higher-order contamination was reduced by using a pyrolitic graphite filter. The final energy was fixed at 14.7 meV. The platelike Nd_2CuO_4 single crystal (~1 g) with a mosaic spread of less than 0.3° was mounted in an Orange He cryostat and kept at a temperature of 4 K. At this temperature the Nd moments are in a paramagneticlike state because they are only weakly polarized by the Nd-Cu exchange interaction. In order to measure the dispersion along all three high-symmetry directions, we had to perform the experiments with two different orientations of the sample; one with the 100 axis vertical and one with the 110 axis vertical.

Only two of the four ground-state transitions were observed in these experiments. The transition at ~14 meV has a very small matrix element and could therefore not be detected. The transition at ~93 meV is out of reach for a thermal neutron spectrometer. We therefore focused on the transitions at ~21 and ~27 meV. There was some controversy in the literature about the symmetry of these two CEF levels. One group claimed that the level at 21 meV has a Γ_6 and the one at 27 meV a Γ_7 representation.[38,57] Another group however recently assigned the level at 21 meV to Γ_7 and the one at 27 meV to a Γ_6 symmetry.[37] Because the ground-state doublet has Γ_6 symmetry, the two cases represent different polarizations for the two CEF transitions. This controversy was resolved by a Raman study of intermultiplet crystal-field excitations in Nd_2CuO_4,[41] where it was found that the level at 21 meV has a Γ_6 representation. It was argued in that paper that the major difficulty of neutron scattering in determining a set of CEF parameters is the limited number of detected levels. We will however show that inelastic neutron-scattering experiments on single crystals give enough information to unambiguously determine the symmetry of the different excitation levels. The neutron cross section for the scattering from the single-ion CEF excitation $|\Gamma_n\rangle\rightarrow|\Gamma_m\rangle$ is given by[58]

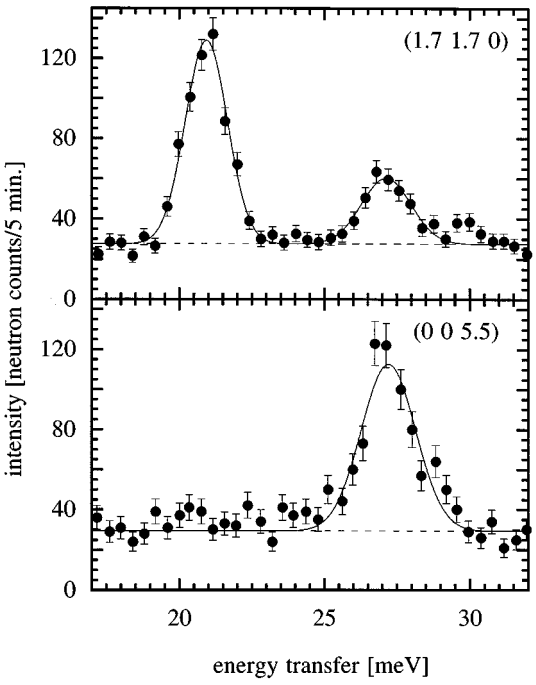

FIG. 2. Energy spectra of neutrons scattered from Nd_2CuO_4 at 4 K for two different $\vec{Q}$ positions.

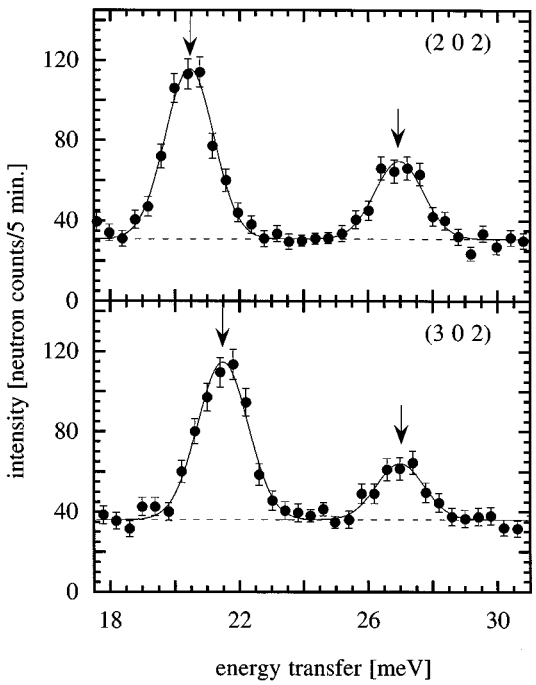

FIG. 3. Energy spectra of neutrons scattered from Nd_2CuO_4 at 4 K for two different $\vec{Q}$ positions.

$$\frac{d^2\sigma}{d\Omega\, d\omega} = N\left(\frac{1}{2} g\gamma r_0\right)^2 \frac{k}{k'} F^2(\vec{Q}) \exp\{-2W(\vec{Q})\} p_{\Gamma_n} \times \sum_\alpha \left(1-\frac{Q_\alpha^2}{Q^2}\right) |\langle \Gamma_m|\hat{J}^\alpha|\Gamma_n\rangle|^2 \delta(\hbar\omega + E_{\Gamma_n} - E_{\Gamma_m}) \tag{1}$$

where N is the total number of magnetic ions, g is the Landé splitting factor, γ is the gyromagnetic ratio of the neutron, $\vec{Q}=\vec{k}-\vec{k}'$ is the scattering vector with $\vec{k}$ and $\vec{k}'$ the wave vectors of the incoming and scattered neutron, respectively, $F(\vec{Q})$ is the magnetic form factor, and $\exp\{-2W(\vec{Q})\}$ is the Debye-Waller factor. E_{Γ_n} and p_{Γ_n} denote the energy and the Boltzmann population factor of the CEF level $|\Gamma_n\rangle$. $\hat{J}^\alpha$ ($\alpha = x,y,z$) stands for the Cartesian component of the total angular momentum operator.

A transition between two Γ_6 levels has longitudinal character, i.e., $\langle n|J_{x,y}|m\rangle = 0$ and $\langle n|J_z|m\rangle \neq 0$, whereas a transition between a Γ_6 and a Γ_7 level has transverse character, i.e., $\langle n|J_{x,y}|m\rangle \neq 0$ and $\langle n|J_z|m\rangle = 0$. The polarization factor $(1-Q_\alpha^2/Q^2)$ in formula (1) allows these cases to be distinguished. Figure 2 shows a measurement at two different positions in reciprocal space. It is obvious that the transition at 21 meV has longitudinal character because it cannot be observed for Q parallel [001]. The transition at 27 meV on the other hand has transverse character. It follows that the level at 21 meV corresponds to a Γ_6 representation, while the level at 27 meV has Γ_7 symmetry.

Inelastic neutron scattering on single crystals does not only give information on the polarization of the CEF transitions, but it also measures directly the $\vec{q}$ dependence of the energies, where we define $\vec{q}$ by $\vec{Q}=\vec{q}+\vec{\tau}$ with $\vec{\tau}$ being a reciprocal-lattice vector. Such a dependence occurs when the magnetic moments of the rare-earth ions are exchange coupled. Figure 3 shows a measurement at two different positions in reciprocal space. It can clearly be seen that the transition at 21 meV shows a pronounced dispersion, while no $\vec{q}$ dependence can be detected for the transition at 27 meV. We therefore focused our attention on the former transition and measured its dispersion along the three main symmetry directions. Because the scattering from this transition is zero for $\vec{Q}=(00l)$ we had to determine the dispersion for the [001] direction at $(11l)$ positions. Figure 4 shows the results of these measurements at four different $\vec{Q}$ vectors. At several positions we observed significant line broadenings and line asymmetries which indicate the presence of two excitation branches. We therefore fitted the data with two Gaussian lines, keeping the linewidth constant according to the experimental resolution. In Fig. 5 we show the resulting intensities of the two different branches at $(11l)$ positions. It can be seen that the two branches continuously interchange intensity. The scattering of the two branches is maximal at $\vec{Q}=(110)$ and near $\vec{Q}\approx(112)$, respectively. Moreover when changing h or k and keeping l equal to 0 or 2, we did not observe any line broadening. This indicates that the relative intensities of the two excitation branches depend on l only, in agreement with theoretical findings as shown later. Therefore, to determine the dispersion along the [100] and [110] direction for both branches, we performed scans at $(hk0)$ and $(hk2)$ positions, respectively. In Fig. 6 we show the measured dispersion of the two excitation branches along the three main symmetry directions. Because the measurements were performed in the paramagnetic state of the Nd spin system, we use the Brillouin zone of the chemical Nd sublattice for the description of the positions in reciprocal space. Figure 1 (upper right) shows the Brillouin zone of the direct body-centered-tetragonal lattice.

To describe the data we made use of the mean-field

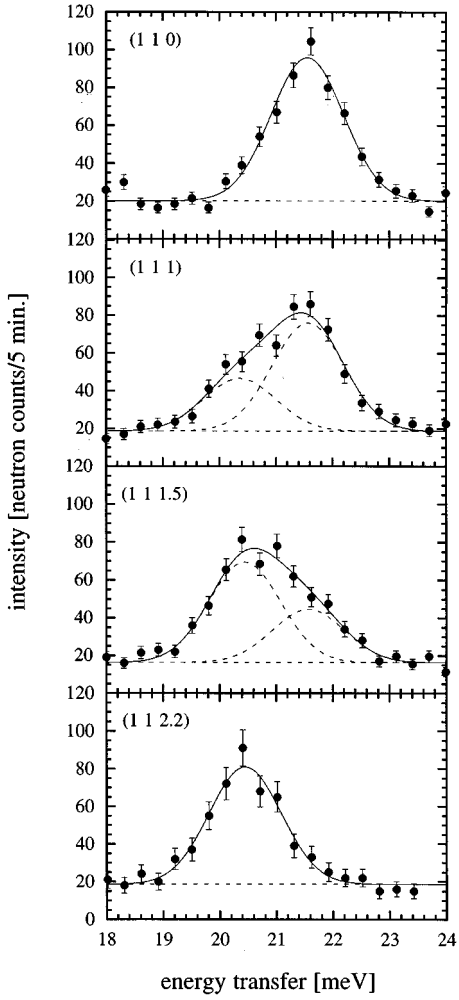

FIG. 4. Energy spectra of neutrons scattered from Nd_2CuO_4 at 4 K for different $\vec{Q}=(11l)$. The lines are the result of least-squares fits as explained in the text.

random-phase approximation (RPA) model, see, e.g., Ref. 59. In principle, one has to include the complete CEF level scheme in the calculation of the dispersion of the $\Gamma_6^{(1)}$-$\Gamma_6^{(2)}$ transition. The transition at 14 meV has, however, a very small matrix element and gives therefore a negligible contribution to the single-ion susceptibility. The $\Gamma_6^{(1)}$-$\Gamma_7^{(1)}$and the $\Gamma_6^{(1)}$-$\Gamma_7^{(2)}$ transitions are moreover de-

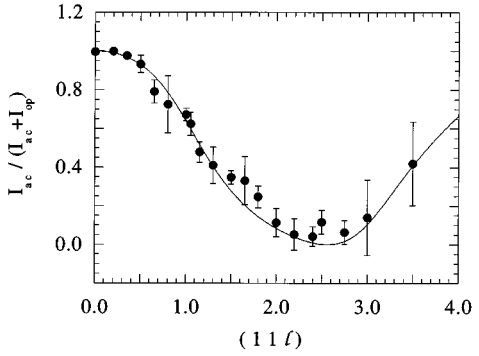

FIG. 5. Measured intensity of the acoustic branch at $(11l)$ positions, normalized to the total magnetic scattering. The line corresponds to the RPA model calculation.

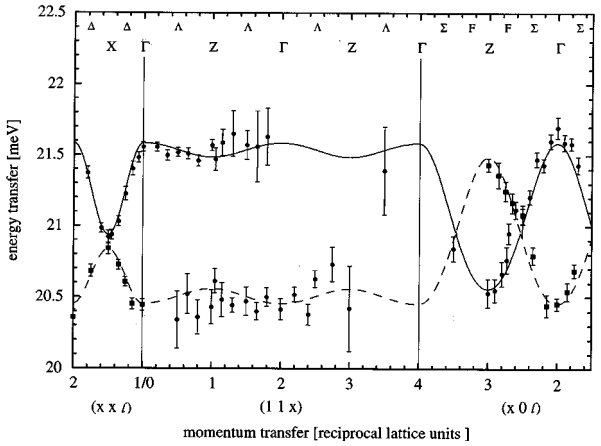

FIG. 6. Measured dispersion of the $\Gamma_6^{(1)}$-$\Gamma_6^{(2)}$ Nd CEF excitation in Nd_2CuO_4 at 4 K (circles: $l=0$, squares: $l=2$). The lines correspond to the RPA model calculation.

coupled from the $\Gamma_6^{(1)}$-$\Gamma_6^{(2)}$ excitation because of the different polarizations. The contribution of the transition at 93 meV is also insignificant because of the large energy difference and the small matrix element. We can therefore calculate the dispersion individually for the $\Gamma_6^{(1)}$-$\Gamma_6^{(2)}$ doublet-doublet excitation. Due to the Cu-Nd exchange field, the ground-state doublet is split by about 0.5 meV, whereas the doublet at 21 meV is split by about 0.3 meV. Only two of the four possible transition matrix elements between the two resulting ground-state singlets at 0 and ~0.5 meV and the two excited singlets at ~21.2 and ~21.5 meV are nonzero. We are left with two singlet-singlet transitions with an energy difference of about 0.2 meV. Within the spectrometer resolution, however, we cannot distinguish these two excitations. Because both excitations are expected to have the same dispersion, we can describe our data in the framework of a singlet-singlet transition.

Because of the two-ion basis of the Nd we assume the spin Hamiltonian to have the following form:[59–61]

$$H=\sum_i V_i^c-\sum_{i>j} J(\vec{r}_i-\vec{r}_j)\vec{J}_i\cdot\vec{J}_j-\sum_{i>k} J'(\vec{r}_i-\vec{r}_k)\vec{J}_i\cdot\vec{J}_k, \tag{2}$$

where V_i^c is the single-ion CEF potential, $J(\vec{r}_i-\vec{r}_j)$ are the intrasublattice exchange constants, and $J'(\vec{r}_i-\vec{r}_k)$ are the intersublattice exchange constants. In the paramagnetic state, at low temperatures, this leads to the following expression for the energy dispersion of a singlet-singlet CEF excitation:[59–61]

$$E(\vec{q})=[\Delta^2-2M^2\Delta\{J(\vec{q})\pm\nu|J'(\vec{q})|\}]^{1/2}, \tag{3}$$

where Δ is the CEF splitting, $M=|\langle\Gamma_6^{(1)}|J_z|\Gamma_6^{(2)}\rangle|=2.60$ is the transition matrix element, $J(\vec{q})$ and $J'(\vec{q})$ are the Fourier transformed coupling constants between ions of the same and of different sublattices, respectively, and $\nu=\pm1$ denotes the sign of $J'(0)$.

The + and − sign in Eq. (3) corresponds to the acoustic and optical branch, respectively. The scattering intensity of the two branches is proportional to[59,60]

$$I \propto M_\alpha^2 \Delta^2 \sum_\alpha (1-Q_\alpha^2)[F(\vec{Q})]^2\{1\pm\cos(\varphi)\}/E(\vec{q}), \quad (4)$$

where $F(\vec{Q})$ is the Nd^{3+} magnetic form factor, and the phase φ is defined through $J'(\vec{Q})=J'(\vec{q})\exp(-i\vec{\tau}\cdot\vec{\rho})=\nu|J'(\vec{q})|\exp(-i\varphi)$, with $\vec{\tau}$ being a reciprocal-lattice vector and $\vec{\rho}$ being the vector connecting the two sublattices.

This model gives a very good description of our data. In Fig. 1 we indicated the coupling constants that were included in the fit procedure. The line drawn in Fig. 6 corresponds to the calculated dispersion. The model predicts that the intensity ratio between the acoustic and the optic branch changes only if l changes, as observed in the experiments. The intensity ratio between these two branches along the [001] direction agrees perfectly with the measurements, as shown in Fig. 5. We derive the following coupling constants for this CEF excitation:

$$J_1=-7\pm2 \ \ \mu\text{eV}, \quad J_2=-19\pm1 \ \ \mu\text{eV},$$

$$J_3=-2.5\pm1 \ \ \mu\text{eV}.$$

It is also obvious from Eq. (3) why we could not observe a $\vec{q}$ dependence for the $\Gamma_6{}^{(1)}$-$\Gamma_7{}^{(2)}$ CEF transition at 27 meV. Using the above exchange parameters and $M=|\langle\Gamma_6^{(1)}|J_{x,y}|\Gamma_7^{(2)}\rangle|=1.74$, the resulting dispersion of less than 0.4 meV cannot be determined with our experimental resolution.

III. Nd SPIN WAVES IN $Nd_{2-x}Ce_xCuO_4$ ($x=0,0.13$)

We performed these experiments on the cold triple-axis spectrometer V2 installed at the reactor BER 2 of the Berlin Neutron Scattering Center (BENSC). We used a vertically curved graphite (002) monochromator and a horizontally bent graphite (002) analyzer. A 40′ collimator and a Be filter, cooled by liquid nitrogen, were installed between monochromator and sample. No collimation was used between sample and detector. All scans were performed with a fixed out-going energy of 3.5 meV. We used the same Nd_2CuO_4 single crystal as in the experiment described in Sec. II. A few energy scans were performed on a Ce-doped $Nd_{1.83}Ce_{0.13}CuO_4$ single crystal. The samples were put into a ^{3}He-^{4}He dilution refrigerator insert and kept at a fixed temperature of 50 mK. At this temperature the Nd spin order is completely saturated. We performed the experiments with two different orientations of the sample; one with the 100 axis vertical and one with the 110 axis vertical.

In Figs. 7 and 8 we show some energy scans performed on the Nd_2CuO_4 compound. Since the noncollinear antiferromagnetic (AF) structure of the Nd spins comprises eight magnetic sublattices, one expects eight spin-wave modes. It is obvious from the spectra shown that the major problem in the data analysis is the identification of the different excitation branches. Such an analysis can only be performed by including a model that predicts the intensities of the different excitation branches at different positions in reciprocal space.

The model calculations were performed in the context of a mean-field RPA approximation. For the present purpose only the $\Gamma_6{}^{(1)}$ ground-state doublet is essential which can be described by a pseudospin $S=1/2$. We define the model by

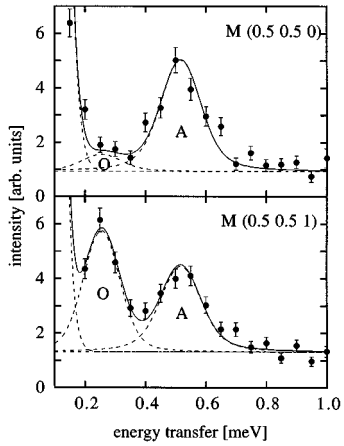

FIG. 7. Energy spectra of neutrons scattered from Nd_2CuO_4 at $T=50$ mK at two different M points. *A* stands for the acoustic, *O* for the optic excitation. The lines are the result of a least-squares fitting procedure as explained in the text.

$$H=-\sum_{i>j} \vec{S}_i I(\vec{r}_i-\vec{r}_j)\vec{S}_j-\sum_i \vec{h}_{\rm Cu}\vec{S}_i. \quad (5)$$

We assume a diagonal Nd-Nd exchange tensor $I_{\alpha\beta}$ ($\alpha,\beta=x,y,z$) where $I_{xx}=I_{yy}=I^\perp$ and $I_{zz}=I^\parallel$ are different because of the anisotropy induced by the CEF potential. This anisotropy is given by $I^\parallel/I^\perp=|\langle\phi_0|J_z|\phi_1\rangle|^2/|\langle\phi_0|J_{x,y}|\phi_1\rangle|^2\approx0.2$, where $|\phi_0\rangle$ and $|\phi_1\rangle$ denote the wave functions of the split ground-state $\Gamma_6{}^{(1)}$ doublet. $\vec{h}_{\rm Cu}$ is the Cu-exchange field acting on the Nd pseudospins. At low temperatures $T\ll T_N[\text{Cu}]$ it has the saturation value $h_{\rm Cu}^0$.

We were able to obtain closed expressions for the spin-wave frequencies in the whole Brillouin zone for arbitrary uniaxial anisotropy of the exchange constants. The eight spin-wave modes consist of four acoustical (A) and four optical (O) branches. The latter should only be visible, if the total momentum transfer $\vec{Q}=(hkl)$ has an $l\neq0$ component, while the A modes can have intensity also for $l=0$. To index the magnetic excitations we used the reciprocal lattice of the magnetic unit cell which is obtained by a $\sqrt{2}\times\sqrt{2}$ expansion and 45° rotation of the chemical unit cell basal plane (Fig. 1, lower right). We give here only the results of the calculation. First we introduce the Fourier functions $\hat{I}_\kappa^\alpha$ of the exchange tensor with $\alpha=\perp,\parallel$ and $\kappa=r,s$:

$$\begin{aligned}\hat{I}_r^\alpha(\vec{q})&=\hat{\pm}I_1^\alpha-2I_2^\alpha\{\cos(\tfrac{1}{2}\hat{q}_y)\tilde{\pm}\cos(\tfrac{1}{2}\hat{q}_x)\}\\&\quad\tilde{\pm}4I_3^\alpha\cos(\tfrac{1}{2}\hat{q}_x)\cos(\tfrac{1}{2}\hat{q}_y)+2I_4^\alpha\{\cos(\hat{q}_x)\\&\quad+\cos(\hat{q}_y)\},\\ \hat{I}_s^\alpha(\vec{q})&=\hat{\pm}I_1^\alpha+2I_2^\alpha\{\cos(\tfrac{1}{2}\hat{q}_y)\tilde{\pm}\cos(\tfrac{1}{2}\hat{q}_x)\}\\&\quad\tilde{\pm}4I_3^\alpha\cos(\tfrac{1}{2}\hat{q}_x)\cos(\tfrac{1}{2}\hat{q}_y)+2I_4^\alpha\{\cos(\hat{q}_x)\\&\quad+\cos(\hat{q}_y)\}\end{aligned} \quad (6)$$

and the function

$$\hat{\beta}^\alpha(\vec{q})=\hat{\pm}8\langle S\rangle\hat{I}_1^\alpha\hat{I}_2^\alpha\{\cos(\tfrac{1}{2}\hat{q}_y)\tilde{\pm}\cos(\tfrac{1}{2}\hat{q}_x)\}\sin^2(\tfrac{1}{4}\hat{q}_z), \quad (7)$$

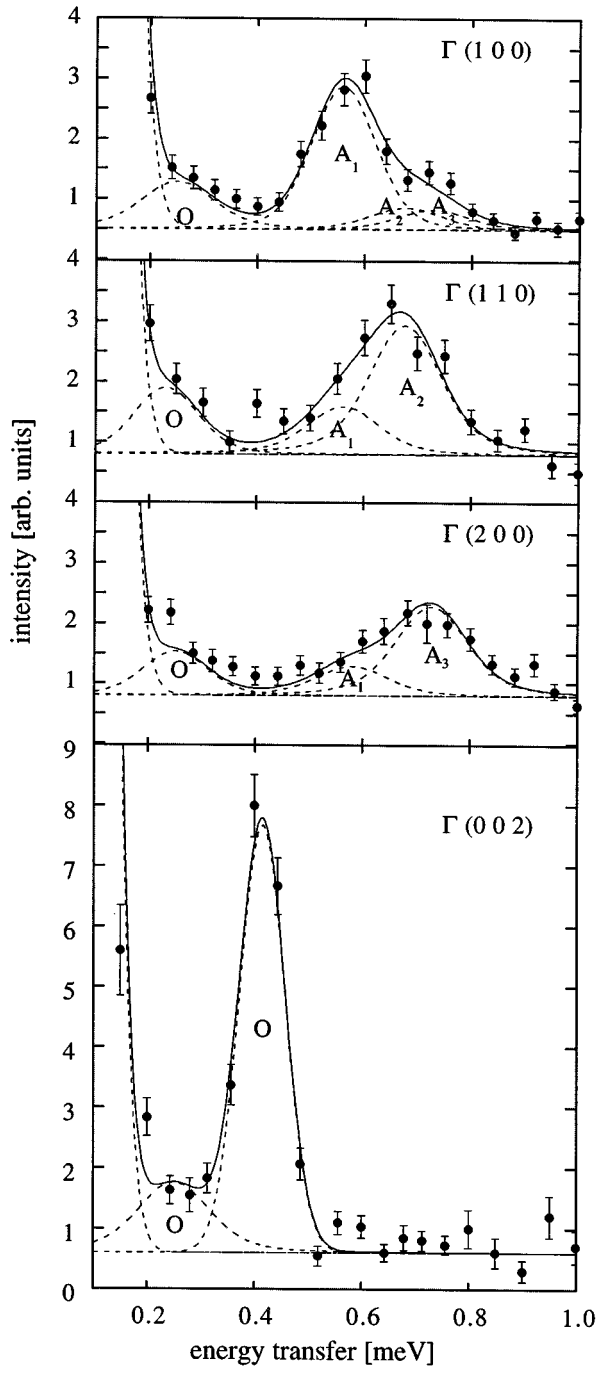

FIG. 8. Energy spectra of neutrons scattered from Nd_2CuO_4 at $T=50$ mK at four different Γ points. For the scans with $l=0$ the intensity ratio was kept fixed according to the model calculation. The three acoustic excitations are denoted by A_1, A_2, and A_3. All the optic excitations are denoted by O.

where $\hat{q}_x=\sqrt{2}aq_x$, etc. Note that q_x, q_y refer to the magnetic Brillouin zone and that a represents the lattice constant of the chemical unit cell. In addition the I_i^α ($\alpha=\perp,\parallel$ and $i=$1-4) are the exchange constants between the Nd ''pseudospins'' of the $\Gamma_6^{(1)}$ ground state at various adjacent sites as defined in Fig. 1 where the extra coupling I_4 used here corresponds to the in-plane diagonal Nd pairs. $\langle S\rangle(\leqslant 1/2)$ denotes the temperature-dependent Nd polarization to be determined self-consistently:

$$\langle S\rangle=\tfrac{1}{2}\tanh\left[\frac{1}{2k_BT}(h_{\mathrm{Cu}}^0+I_{\mathrm{mf}}^\perp\langle S\rangle)\right] \tag{8}$$

with $I_{\mathrm{mf}}^\perp=I_1^\perp-4I_3^\perp+4I_4^\perp$. Note that in Eqs. (6) and (7) $\hat{\pm}$ and $\tilde{\pm}$ signs have to be chosen identically at each place where they occur. Then we define

$$\begin{aligned}
\omega_\kappa^\alpha(\vec{q})&=\Delta-\langle S\rangle\hat{I}_\kappa^\alpha(\vec{q}),\\
\omega_\kappa(\vec{q})&=[\omega_\kappa^\perp(\vec{q})\omega_\kappa^\parallel(\vec{q})]^{1/2},\\
\omega^\alpha(\vec{q})&=[\omega_r^\alpha(\vec{q})\omega_s^\alpha(\vec{q})]^{1/2},\\
\hat{\beta}(\vec{q})&=[\hat{\beta}^\perp(\vec{q})\hat{\beta}^\parallel(\vec{q})]^{1/2}.
\end{aligned} \tag{9}$$

Here Δ is the splitting of the $\Gamma_6^{(1)}$ ground state due to the combined Cu and Nd-exchange field. The latter is given by $I_{\mathrm{mf}}^\perp\langle S\rangle$. The splitting Δ corresponds roughly to the center of spin-wave bands. For wave vector $\vec{q}$ in the tetragonal *ab* plane the eight spin-wave branches are simply given by $\omega_\kappa(\vec{q})$. For general $\vec{q}$ the q_z dispersion enters through the $\hat{\beta}^\alpha(\vec{q})$ functions which mix the in-plane solutions $\omega_\kappa(\vec{q})$ to the general solution $\Omega(\vec{q})$ according to

$$\begin{aligned}
\Omega(\vec{q})=&\tfrac{1}{2}\{\omega_r(\vec{q})^2+\omega_s(\vec{q})^2\}-\hat{\beta}(\vec{q})\\
&\pm[\tfrac{1}{4}\{\omega_r(\vec{q})^2-\omega_s(\vec{q})^2\}^2\\
&-\hat{\beta}(\vec{q})\{\omega_r(\vec{q})^2+\omega_s(\vec{q})^2\}\\
&-\hat{\beta}^\perp(\vec{q})\omega^\parallel(\vec{q})^2-\hat{\beta}^\parallel(\vec{q})\omega^\perp(\vec{q})^2]^{1/2}.
\end{aligned} \tag{10}$$

Equations (6)–(10) constitute the complete spin-wave solution of the noncollinear eight sublattice AF with uniaxial anisotropy. The *A*-*O* splitting of modes is mostly determined by I_1 and to a lesser extent by I_2 which couple the two different chemical sublattices, whereas I_3, I_4 are couplings between various magnetic species of the same chemical sublattice and contribute to the dispersion of spin waves. The dispersion along the q_z direction is caused by terms $\sim I_1I_2$ according to Eq. (7). From these expressions we can derive the degeneracies of the spin-wave modes. They are identical for A,O modes and only the former will be given; Γ point: $2A(1),A(2)$; X point: $2A(2)$; M point: $A(4)$; Z point: $2A(2)$; A point: $A(4)$. Here the first number denotes the multiplicity and the number in brackets denotes the degeneracy. Furthermore along the Λ direction there are two (A and O) doubly degenerate modes which are completely dispersionless. Along the MA direction all modes collapse into two dispersionless fourfold degenerate A,O modes as at the M point. It should be noted that the above spin-wave dispersion for general $\vec{q}$ becomes much simpler for the isotropic ($I^\parallel=I^\perp$) case.[62]

For the case with $l=0$ the polarization vectors of spin-wave modes can easily be obtained which also allowed us to compute their structure factors whose explicit expressions will be given elsewhere.[62] The calculated intensities turned out to be only weakly dependent on the size of the exchange parameters. In a first step we calculated the intensities with the help of the coupling constants obtained for the $\Gamma_6^{(1)}-\Gamma_6^{(2)}$ CEF excitations. They have been used in the following to analyze the intensity of the observed acoustic modes

for $l=0$ momentum transfer. The intensities finally calculated with the coupling parameters for the spin-wave excitations only differed by a few percents from these values.

In Figs. 7 and 8 we show the results at the M and Γ point, respectively. The $\vec{Q}$ vectors are given in reciprocal-lattice units of the magnetic unit cell. All the excitations were fitted by a damped harmonic oscillator shape convoluted with the resolution function of the spectrometer. The intrinsic energy width was typically 0.03 meV. The model calculation reveals that there are two fourfold degenerate excitations present at the M point, an acoustic and an optic one. For $l=0$, only the acoustic excitation should be detectable. For $l\neq 0$ the optic excitation should appear in the spectra. We saw indeed that both excitations are clearly visible at (0.5, 0.5, 1). The optic excitation is however already detectable at (0.5, 0.5, 0). We found that for all the scans performed with $l=0$ there is some scattering intensity visible at $\sim$0.25 meV. We concluded that this scattering is due to a flat optical excitation branch that can be detected for $l=0$ because of the limited $\vec{Q}$ resolution. This interpretation is supported by the fact that experiments on powder samples indicate the existence of such a flat excitation branch at $\sim$0.25 meV.[40]

At the Γ point the calculation shows that there are six excitations present, two of them twofold degenerate. The intensities of the acoustic branches strongly depend on the chosen reciprocal-lattice vector. In the fits shown in Figs. 8(a)–8(c) we fixed the intensity ratio of the acoustic modes to the calculated value. In this way it was possible to determine the energies of the three acoustic modes unambiguously. As mentioned before, in all these spectra we also detected an optic branch at $\sim$0.25 meV. As soon as we went to nonzero l, for example (002), we could then detect a second optical branch. The excitations of the third optical branch were not visible for any of the chosen l.

For all the other points in reciprocal space we proceeded in the same manner. Although we performed scans at over 60 different positions in reciprocal space, we could not completely determine the dispersion for all the branches. Due to kinematic constraints, it was not possible to measure at l values higher than $\approx$4.5. Moreover, the intensity drastically decreases for large $\vec{Q}$ because of the magnetic form factor of Nd.

The obtained information is, however, more than sufficient to determine the four exchange constants that we included in the calculation. In Fig. 9 we show the measured and calculated dispersion relations. The resulting exchange constants $I_i^{\perp}$ and the splitting h_{Cu}^0 of the Nd ground-state doublet due to the Nd-Cu exchange are as follows:

$$I_1^{\perp}=-0.43\pm0.03\ \text{meV},\quad I_2^{\perp}=-0.06\pm0.01\ \text{meV},$$

$$I_3^{\perp}=-0.07\pm0.01\ \text{meV},$$

$$I_4^{\perp}=-0.04\pm0.01\ \text{meV},\quad h_{\mathrm{Cu}}^0=0.63\pm0.03\ \text{meV}.$$

The exchange couplings I_i obtained for pseudospins $S=1/2$ can be transformed into the exchange couplings J_i corresponding to the Hamiltonian (2) expressed in the total angular momentum operator $\hat{J}$ via $J_i=I_i^{\perp}/4|\langle\phi_0|\hat{J}_{x,y}|\phi_1\rangle|^2=I^{\perp}/13.50$. We then obtain for the exchange couplings of the Nd moments the following values:

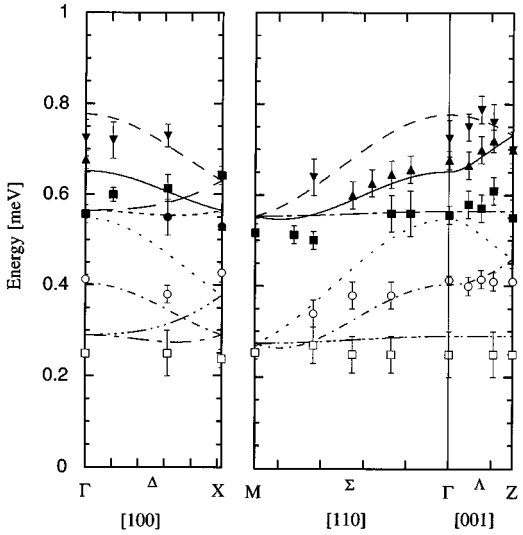

FIG. 9. Measured dispersion of the Nd spin waves in Nd_2CuO_4 at $T=50$ mK. The lines correspond to the model calculation with the exchange constants given in the text. Note that the dispersion along [001] is slightly changed compared to Ref. 56 where the degeneracy at Z was not given correctly.

$$J_1=-32\pm2\ \ \mu\text{eV},\quad J_2=-4\pm1\ \ \mu\text{eV},$$

$$J_3=-5\pm1\ \ \mu\text{eV},\quad J_4=-3\pm1\ \ \mu\text{eV}.$$

Finally, we show some preliminary results of our measurement on a Ce-doped $Nd_{1.87}Ce_{0.13}CuO_4$ single crystal. In Fig. 10 we compare a spectrum of this compound with that taken on the pure Nd_2CuO_4 compound at the same temperature and the same position in reciprocal space. The lines

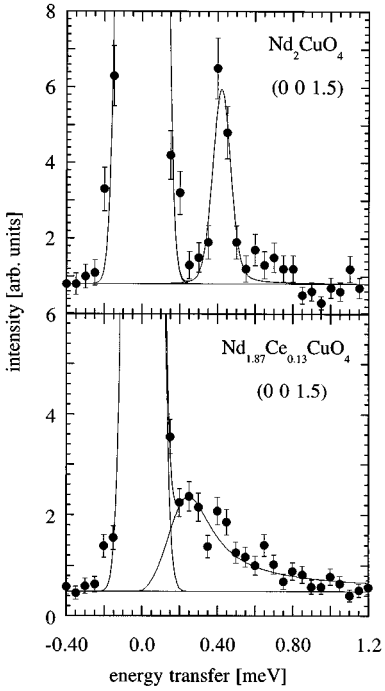

FIG. 10. Energy spectra of neutrons scattered from Nd_2CuO_4 and $Nd_{1.87}Ce_{0.13}CuO_4$ at 50 mK for $\vec{Q}=(0\,0\,1.5)$. The line corresponds to least-squares fits as explained in the text.

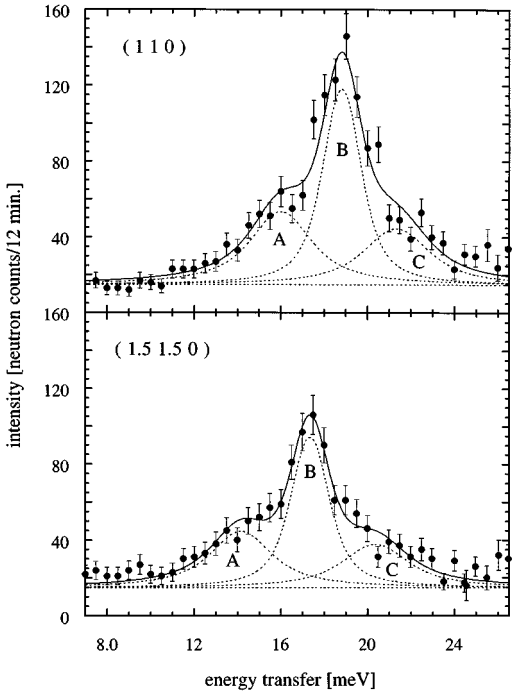

FIG. 11. Energy spectra of neutrons scattered from $Pr_{1.86}Ce_{0.14}CuO_4$ at 10 K at the two different $\vec{Q}$ positions (1 1 0) and (1.5 1.5 0).

correspond to least-squares fits with a damped harmonic oscillator shape corrected with the detailed balance factor and convoluted with the resolution function. One observes a renormalization of the energy in the Ce-doped sample which is most probably due to the reduction of the Cu magnetic moment induced by the doping process, which reduces h_{Cu}. Moreover, there is also a pronounced line broadening present in the doped compound. We will further discuss these findings in Sec. V.

IV. DISPERSION OF THE Γ_4-Γ_5 Pr CEF EXCITATION IN $Pr_{1.86}Ce_{0.14}CuO_4$

The investigation of the dispersion of the Γ_4-Γ_5 CEF excitation was performed on the spectrometer IN3 at the Institut Laue-Langevin in Grenoble. We used the same spectrometer configuration as described in Sec. II. The $Pr_{1.86}Ce_{0.14}CuO_4$ single crystal was mounted in a closed-cycle refrigerator and kept at a temperature of 12 K. The experiments were performed in two configurations with the 100 axis vertical and the 110 axis vertical, respectively.

Figure 11 shows the results of the measurements at two different positions in reciprocal space. It has been shown in an inelastic neutron-scattering study on $Pr_{2-x}Ce_xCuO_4$ ($0 \leqslant x \leqslant 0.2$) powder samples[63] and in a Raman crystal-field study on a $Pr_{1.85}Ce_{0.15}CuO_4$ single crystal[64] that the observed energy spectra in these compounds result from a superposition of different components whose spectral weights strongly depend on the doping level. The reason for this is the formation of local clusters which correspond to different doping levels. For $x \approx 0.14$, one expects three main contributions to the scattering originating from excitations at $\approx$15 meV (A), $\approx$18 meV (B), and $\approx$21 meV (C). We therefore performed

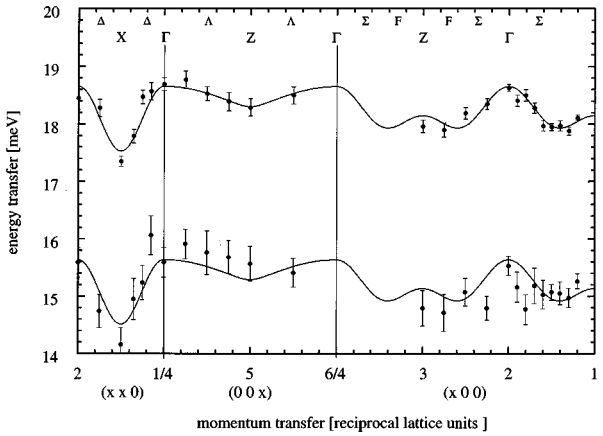

FIG. 12. Measured dispersion of the acoustic branch of the Γ_4-Γ_5 Pr CEF excitation in $Pr_{1.86}Ce_{0.14}CuO_4$ at 10 K. The lines correspond to the RPA model calculation as explained in the text.

the data treatment in the following way. We fitted the spectra with three individual excitations with line shapes representing a damped harmonic oscillator line convoluted with the resolution function. The intensity ratio of the different excitations was kept fixed according to the ratios established in the experiments on powder samples. The result of this fitting procedure is shown in Fig. 11. It can be seen that the energy of excitation B is very well defined. The energy of excitation A can also be quite accurately determined, while the energy of excitation C is not well determined. In Fig. 12 we show the measured dispersion for the excitations marked with A and B along the three main symmetry directions.

To describe the data we made use of the mean-field random-phase approximation (RPA) model as outlined in Sec. II. This model has successfully been applied to describe the dispersion of the Γ_4-Γ_5 CEF excitation of Pr in Pr_2CuO_4.[30] In our case, because of the dilution of the Pr spin system, the coupling corresponds only to an effective spin exchange interaction which is reduced in comparison with the actual exchange coupling. Moreover, it is not clear whether we can use this model individually for each of the three excitations A, B, and C. The decomposition of the spectra into three individual excitations has its origin in the presence of different CEF surroundings on a local scale. The corresponding cluster sizes are presumably of the order of 6 Å, as observed in $Nd_{2-x}Ce_xCuO_4$ ($x=0.165$ and 0.2) by real-space refinement of neutron powder diffraction.[65] The dispersion of the spin excitations on the other hand is a cooperative effect with a typical coherence length of the order of 100 Å. It is therefore difficult to develop a model that takes into account the local inhomogeneities. Applying the RPA description for each individual excitation is however a good approximation if we assume that the exchange couplings between all the ions are identical, regardless of their CEF surroundings.

It was demonstrated in Ref. 30 that it is very difficult to measure the dispersion of the optic branch in the Pr_2CuO_4 compound. At positions with $4 \leqslant l \leqslant 6$, where we measured the dispersion along [001], the contribution of the optic branch to the total scattering varies between $\sim$0 and $\sim$30 %. In the case of the doped sample where the magnetic scattering is split into three excitations it was therefore impossible

TABLE I. Exchange coupling constants in Nd_2CuO_4, Pr_2CuO_4 (Ref. 30), and $Pr_{1.86}Ce_{0.14}CuO_4$ derived from the dispersion of the CEF excitations. In the case of Nd_2CuO_4, (1) stands for the exchange coupling obtained for the low-energy spin waves and (2) for the couplings obtained for the $\Gamma_6^{(1)}$-$\Gamma_6^{(2)}$ Nd CEF excitation.

	Nd_2CuO_4 (1)	Nd_2CuO_4 (2)	Pr_2CuO_4	$Pr_{1.86}Ce_{0.14}CuO_4$
J_1 (μeV)	-32 ± 2	-7 ± 2	-50 ± 5	-30 ± 10
J_2 (μeV)	-4 ± 1	-19 ± 1	-15 ± 2	-10 ± 2
J_3 (μeV)	-5 ± 1	-2.5 ± 1	-15 ± 2	-16 ± 2
J_4 (μeV)	-3 ± 1			

to determine the $\vec{q}$ dependence of the optic branch. The dispersion shown in Fig. 12 therefore represents the acoustic branch along [100] and [110] for the two excitations *A* and *B*. Along [001], the drawn dispersion is not purely acoustic, because at these positions in reciprocal space there is also some scattering of the optic branch present.

The line drawn in Fig. 12 corresponds to a fit with the acoustic branch given in Eq. (3) where we included the exchange couplings indicated in Fig. 1. We ignored the [001] direction in the fit procedure. However, the dispersion of excitation *B* along [001] corresponds very well to the calculated dispersion of the acoustic branch. This is due to the fact that the optic excitation associated with the peak *B* occurs at lower energy and presumably is superimposed to peak *A*. This also explains the slight energy offset of the measured dispersion of excitation *A* along [001] compared to the calculation. The coupling constants that we derive from the fitting procedure are the following:

$$M^2J_1=-0.18\pm0.03\ \text{meV},\quad M^2J_2=-0.07\pm0.02\ \text{meV},$$

$$M^2J_3=-0.11\pm0.02\ \text{meV},$$

where $M=|\langle\Gamma_4|J_{x,y}|\Gamma_5\rangle|=2.63$.[36]

V. DISCUSSION

In Table I we summarize the results of our investigation and moreover compare it with the findings in Ref. 30 on Pr_2CuO_4. One can draw the following conclusions:

(1) The doping of Ce ions into Pr_2CuO_4 slightly reduces the exchange couplings. In a first approximation one would expect a reduction of 7% according to the fraction of substituted Pr ions in $Pr_{1.86}Ce_{0.14}CuO_4$. The coupling that is mostly affected by doping is the exchange J_1 mediated by the copper-oxide planes. Because of the big errors it is, however, not reasonable to deduce from that an influence of the electrons in the copper-oxide planes on the exchange interaction. Nevertheless, our results indicate that we would not expect a drastic change of the exchange coupling upon Ce doping in the related $Nd_{2-x}Ce_xCuO_4$ compounds.

(2) The comparison of the exchange couplings for the $\Gamma_6^{(1)}$-$\Gamma_6^{(2)}$ CEF excitation with the coupling parameters derived from the measurements of the spin-wave excitations shows that the exchange interaction is dependent on the initial and the final state of the CEF excitation, i.e., the exchange interaction has to be regarded as a tensor $J_{ij}(\sigma_i,\sigma_j,\sigma_i',\sigma_j')$ where σ denotes the initial and σ' the final state of a CEF excitation. This has so far only been observed in the dimer compound $Cs_3Ho_2Br_9$.[66]

(3) The exchange couplings derived for the Nd ground-state doublet have an interesting property. The mean-field created by the Nd-Cu exchange interaction (+0.63 meV) is directed opposite to the exchange field created by the Nd-Nd exchange interaction (−0.19 meV), see also Ref. 48. This implies that the observed magnetic order of the Nd spins in Nd_2CuO_4 is enforced by the Cu-Nd exchange. The Nd spins themselves would prefer an antiferromagnetic arrangement along the *c* direction. This leads us to argue about the consequences for the Ce-doped samples. There are two effects when doping with Ce ions. Firstly, the replacement of the trivalent Nd ions by the tetravalent nonmagnetic Ce ions dilutes the magnetic Nd sublattice. Secondly, the doping of electrons into the copper-oxide planes reduces the moment of the Cu spins, as revealed by neutron-diffraction measurements. However, such an experiment only gives information on the site-averaged moment. In reality the Cu spin system seems to become highly inhomogeneous upon electron doping. In NMR experiments one observes a superposition of different Cu signals.[67] Our results on the Ce-doped single crystal also indicate the presence of different Cu spin moments, which produce different exchange fields at different Nd sites and consequently lead to the observed line broadening. A detailed theoretical investigation of this scenario would therefore require a proper inclusion of these disorder effects. We will nevertheless try to give an approximation by assuming a ''virtual crystal'' (VC) picture, where we only include the effect of the reduction of the average Cu moments (see, e.g., Ref. 50) and therefore of the average exchange field h_{Cu}. This shifts the Nd spin-wave modes to lower energies as experimentally verified (see Fig. 10 and Ref. 68). In this VC picture, the lowest optical mode shows a complete softening at an incommensurate position close to the *M* point at a critical value $h_{\mathrm{Cu}}/h_{\mathrm{Cu}}^0\approx0.7$. This softening signifies an instability of the Nd spin system, because the Nd moments now tend to an antiferromagnetic alignment along the *c* axis, in contrast to the ferromagnetic alignment induced by the Nd-Cu exchange interaction, which follows from the fact that the soft mode is optical due to $J_1<0$. For values of h_{Cu} below this critical value, one expects for the VC an ordering of the Nd spin system in a new spin arrangement. But because of the effect of disorder the spin-wave spectrum will not recover a finite gap upon further doping as is indeed observed in the results on polycrystalline samples,[68] and consequently one expects a softening of the spin-wave modes in a finite *q* region. This will nevertheless lead to a tendency of the spins to arrange antiferromagnetically along the *c* axis, which could explain the observation of $(h/2,k/2,l/2)$ type magnetic peaks in a $x=0.17$ compound.[50] Moreover, the steep increase of the low-temperature specific heat observed for $x\approx0.1$ could also be due to this softening because it would give rise to a finite density of states of Nd spin excitations even at zero energies.[69] The verification of this scenario requires however further experimental efforts, like the investigation of the expected optical mode softening on single crystals close to the critical concentration $x=0.1$.

ACKNOWLEDGMENTS

We wish to thank Dr. M. Zolliker, Dr. M. Meissner, and H. Schneider for their technical assistance. P.T. is grateful to A. Metz for important suggestions. Financial support by the Swiss National Science Foundation and the Max-Planck-Gesellschaft is gratefully acknowledged. The experiments at BENSC were supported by the European Commission through the Human Capital and Mobility program.

[1] Y. Tokura, H. Takagi, and S. Uchida, Nature (London) **337**, 345 (1989).
[2] H. Takagi, S. Uchida, and Y. Tokura, Phys. Rev. Lett. **62**, 1197 (1989).
[3] O. K. Singh, B. D. Padalia, O. Prakash, K. Suba, A. V. Narlikar, and L. C. Gupta, Physica C **219**, 156 (1994).
[4] M. Brinkmann, T. Rex, H. Bach, and K. Westerholt, Phys. Rev. Lett. **74**, 4927 (1995).
[5] H. Müller-Buschbaum and W. Wollschläger, Z. Anorg. Allg. Chem. **414**, 76 (1975).
[6] R. SaezPuche, M. Norton, T. R. White, and W. S. Glaunsinger, J. Solid State Chem. **50**, 281 (1983).
[7] C. L. Saeman, N. Y. Ayoub, T. Bjornholm, E. A. Early, S. Ghamaty, B. W. Lee, J. T. Markert, J. J. Neumeier, P. K. Tsai, and M. B. Maple, Physica C **159**, 391 (1989).
[8] M. J. Rosseinsky and K. Prassides, Physica C **162-164**, 522 (1989).
[9] D. E. Cox, A. I. Goldman, M. A. Subramanian, J. Gopalakrishnan, and A. W. Sleight, Phys. Rev. B **40**, 6998 (1989).
[10] P. Allenspach, S.-W. Cheong, A. Dommann, P. Fischer, Z. Fisk, A. Furrer, H. R. Ott, and B. Rupp, Z. Phys. B **77**, 185 (1989).
[11] S. Skanthakumar, H. Zhang, T. W. Clinton, W.-H. Li, J. W. Lynn, Z. Fisk, and S.-W. Cheong, Physica C **160**, 124 (1989).
[12] J. Akimitsu, H. Sawa, T. Kobayashi, H. Fujiki, and Y. Yamada, J. Phys. Soc. Jpn. **58**, 2646 (1989).
[13] Y. Endoh, M. Matsuda, K. Yamada, K. Kakurai, Y. Hidaka, G. Shirane, and R. J. Birgeneau, Phys. Rev. B **40**, 7023 (1989).
[14] T. R. Thurston, M. Matsuda, K. Kakurai, K. Yamada, Y. Endoh, R. J. Birgeneau, P. M. Gehring, Y. Hidaka, M. A. Kastner, T. Murakami, and G. Shirane, Phys. Rev. Lett. **65**, 263 (1990).
[15] M. Matsuda, K. Yamada, K. Kakurai, H. Kadowaki, T. R. Thurston, Y. Endoh, Y. Hidaka, R. J. Birgenau, M. A. Kastner, P. M. Gehring, A. H. Moudden, and G. Shirane, Phys. Rev. B **42**, 10 098 (1990).
[16] H. Yoshizawa, S. Mitsuda, H. Mori, Y. Yamada, T. Kobayashi, H. Sawa, and J. Akimitsu, J. Phys. Soc. Jpn. **59**, 428 (1990).
[17] S. Skanthakumar and J. W. Lynn, Physica C **170**, 175 (1990).
[18] S. Skanthakumar, H. Zhang, T. W. Clinton, I. W. Sumarlin, W.-H. Li, J. W. Lynn, Z. Fisk, and S.-W. Cheong, J. Appl. Phys. **67**, 4530 (1990).
[19] T. Chattopadhyay, P. J. Brown, and U. Köbler, Physica C **177**, 294 (1991).
[20] M. J. Rosseinsky, K. Prassides, and P. Day, Inorg. Chem. **30**, 2680 (1991).
[21] A. G. Gukasov, S. Y. Kokovin, V. P. Plakhty, I. A. Zobkalo, S. N. Barilo, and D. I. Zhigunov, Physica B **180 & 181**, 455 (1992).
[22] S. Skanthakumar, J. W. Lynn, J. L. Peng, and Z. Y. Li, J. Magn. Magn. Mater. **104-107**, 519 (1992).
[23] D. Petitgrand, L. Boudarène, P. Bourges, and P. Galez, J. Magn. Magn. Mater. **104-107**, 585 (1992).
[24] G. M. Luke, L. P. Le, B. J. Sternlieb, Y. J. Uemura, J. H. Brewer, R. Kadono, R. F. Kiefl, S. R. Kreitzman, T. M. Riseman, C. E. Stronach, M. R. Davis, S. Uchida, H. Takagi, Y. Tokura, Y. Hidaka, T. Murakami, J. Gopalakrishnan, A. W. Sleight, M. A. Subramanian, E. A. Early, J. T. Markert, M. B. Maple, and C. L. Saeman, Phys. Rev. B **42**, 7981 (1990).
[25] J. Akimitsu, J. Amano, M. Yoshinari, and M. Kokubun, Hyperfine Interact. **85**, 187 (1994).
[26] A. A. Stepanov, M. I. Kobets, V. A. Pashchenko, A. I. Zvyagin, D. I. Zhigunov, and S. N. Barilo, Sov. J. Low Temp. Phys. **17**, 416 (1991).
[27] A. S. Cherny, E. N. Khats'ko, G. Chouteau, J. M. Luois, A. A. Stepanov, P. Wyder, S. N. Barilo, and D. I. Zhigunov, Phys. Rev. B **45**, 12 600 (1992).
[28] S. Skanthakumar, J. W. Lynn, J. L. Peng, and Z. Y. Li, Phys. Rev. B **47**, 6173 (1993).
[29] S. Skanthakumar, J. W. Lynn, J. L. Peng, and Z. Y. Li, J. Appl. Phys. **73**, 6326 (1993).
[30] I. W. Sumarlin, J. W. Lynn, T. Chattopadhyay, S. N. Barilo, and D. I. Zhigunov, Phys. Rev. B **51**, 5824 (1995).
[31] P. E. Sulewski, P. A. Fleury, K. B. Lyons, S.-W. Cheong, and Z. Fisk, Phys. Rev. B **41**, 225 (1990).
[32] V. L. Sobolev, H. L. Huang, Y. G. Pashkevich, M. M. Larionov, I. M. Vitebsky, and V. A. Blinkin, Phys. Rev. B **49**, 1170 (1994).
[33] P. Bourges, A. S. Ivanov, D. Petitgrand, J. Rossat-Mignod, and L. Boudarene, Physica B **186**, 925 (1993).
[34] A. S. Ivanov, P. Bourges, D. Petitgrand, and J. Rossat-Mignod, Physica B **213**, 60 (1995).
[35] P. Allenspach, A. Furrer, R. Osborn, and A. D. Taylor, Z. Phys. B **85**, 301 (1991).
[36] A. T. Boothroyd, S. M. Doyle, D. McK. Paul, and R. Osborn, Phys. Rev. B **45**, 10 075 (1992).
[37] C. K. Loong and L. Soderholm, Phys. Rev. B **48**, 14 001 (1993).
[38] U. Staub, P. Allenspach, A. Furrer, H. R. Ott, S.-W. Cheong, and Z. Fisk, Solid State Commun. **75**, 431 (1990).
[39] P. Hoffmann, M. Loewenhaupt, S. Horn, P. v. Aken, and H.-D. Jostarndt, Physica B **163**, 10 075 (1992).
[40] M. Loewenhaupt, P. Fabi, S. Horn, P. v. Aken, and A. Severing, J. Magn. Magn. Mater. **140-144**, 1293 (1995).
[41] S. Jandl, P. Dufour, T. Strach, T. Ruf, M. Cardona, V. Nekvasil, C. Chen, and B. M. Wanklyn, Phys. Rev. B **52**, 15 558 (1995).
[42] M. F. Hundley, J. D. Thompson, S.-W. Cheong, Z. Fisk, and S. B. Oseroff, Physica C **158**, 102 (1989).
[43] S. Ghamaty, B. W. Lee, J. T. Markert, A. E. Early, T. Bjornholm, C. L. Saeman, and M. B. Maple, Physica C **160**, 217 (1989).
[44] M. B. Maple, N. Y. Ayoub, T. Bjornholm, E. A. Early, S. Ghamaty, B. W. Lee, J. T. Markert, J. J. Neumeier, and C. L. Saeman, Physca, C **162-164**, 296 (1989).
[45] J. W. Lynn, I. W. Sumarlin, S. Skanthakumar, W.-H. Li, R. N. Shelton, J. L. Peng, Z. Fisk, and S.-W. Cheong, Phys. Rev. B **41**, 2569 (1990).

[46] J. P. Hill, A. Vigliante, D. Gibbs, J. L. Peng, and R. L. Greene, Phys. Rev. B **52**, 6575 (1995).
[47] A. T. Boothroyd, S. M. Doyle, D. M. Paul, D. S. Misra, and R. Osborn, Physica C **165**, 17 (1990).
[48] P. Adelmann, R. Ahrens, G. Czjek, G. Roth, H. Schmidt, and C. Steinleitner, Phys. Rev. B **46**, 3619 (1992).
[49] T. Chattopadhyay and K. Siemensmeyer, Europhys. Lett. **29**, 579 (1995).
[50] S. Skanthakumar, Ph.D. thesis, University of Maryland, 1993.
[51] T. Brugger, T. Schreiner, G. Roth, P. Adelmann, and G. Czjzek, Phys. Rev. Lett. **71**, 2481 (1993).
[52] P. Fulde, V. Zevin, and G. Zwicknagl, Z. Phys. B **92**, 133 (1993).
[53] J. Igarashi, T. Tonegawa, M. Kaburagi, and P. Fulde, Phys. Rev. B **51**, 5814 (1995).
[54] J. Igarashi, K. Murayama, and P. Fulde, Phys. Rev. B **52**, 15 966 (1995).
[55] W. Henggeler, T. Chattopadhyay, B. Roessli, D. I. Zhigunov, S. N. Barilo, and A. Furrer, Z. Phys. B **99**, 465 (1996).
[56] W. Henggeler, T. Chattopadhyay, P. Thalmeier, P. Vorderwisch, and A. Furrer, Europhys. Lett. **34**, 537 (1996).
[57] A. Furrer, P. Allenspach, J. Mesot, and U. Staub, Physica C **168**, 609 (1990).
[58] G. T. Trammel, Phys. Rev. **92**, 1387 (1953).
[59] J. Jensen and A. R. Mackintosh, *Rare Earth Magnetism, Structures and Excitations* (Oxford Science, Clarendon, Oxford, 1991).
[60] P. A. Lindgård and J. G. Houmann, *Rare Earths and Actinides* (Institute of Physics, London, 1971).
[61] J. G. Houmann, M. Chapellier, A. R. Mackintosh, P. Bak, O. D. McMasters, and K. A. Gschneidner, Phys. Rev. Lett. **34**, 587 (1975).
[62] P. Thalmeier, Physica C **266**, 89 (1996).
[63] W. Henggeler, G. Guntze, M. Klauda, J. Mesot, A. Furrer, and G. Saemann-Ischenko, Europhys. Lett. **29**, 233 (1995).
[64] J. A. Sanjurjo, G. B. Martins, P. G. Pagliuso, E. Granado, I. Torriani, C. Rettori, S. Oseroff, and Z. Fisk, Phys. Rev. B **51**, 1185 (1995).
[65] S. J. L. Billinge and T. Egami, Phys. Rev. B **47**, 14 386 (1993).
[66] A. Furrer, H. U. Güdel, E. R. Krausz, and H. Blank, Phys. Rev. Lett. **64**, 68 (1990).
[67] M. Abe, K. Kumagai, S. Awaji, and T. Fujita, Physica C **160**, 8 (1989).
[68] M. Loewenenhaupt, A. Metz, N. M. Pyka, D. McK. Paul, J. Martin, V. H. M. Duijn, J. J. M. Franse, H. Mutka, and W. Schmidt, Ann. Phys. **5**, 197 (1996).
[69] P. Thalmeier, Physica B (to be published).